Available online at www.sciencedirect.com
SCIENCE DIRECT®
Acta Materialia 53 (2005) 705–717
Acta MATERIALIA
www.actamat-journals.com

Hardness and plastic deformation in a bulk metallic glass

U. Ramamurty [a,*], S. Jana [a], Y. Kawamura [b], K. Chattopadhyay [a]

[a] Department of Metallurgy, Indian Institute of Science, Bangalore 560 012, India
[b] Department of Mechanical Engineering and Materials Science, Kumamoto University, 2-39-1 Kurokami, Kumamoto 860-8555, Japan

Received 11 July 2004; received in revised form 11 October 2004; accepted 14 October 2004
Available online 11 November 2004

Abstract

An experimental investigation into the Vickers hardness and associated plastic deformation in as-cast and annealed $Pd_{42}Ni_{40}P_{18}$ bulk metallic glass was conducted. In addition to the bulk indentation behavior, the deformation morphology underneath the indenter and its variation with annealing time was examined by employing the bonded interface technique. For both the bulk and the interface indentations, the trends in the shear band induced plastic deformation zone sizes with the indentation load agree well with those predicted from the expanding cavity model. However, the yield strength extracted from the indentation data is higher than that measured in uniaxial compression, indicating pressure sensitive plasticity. Results show that the as-cast as well as the partially crystallized alloys deform appreciably through the shear band mechanism, with semi-circular and radial shear band morphologies. The latter gets increasingly prominent with increasing annealing time. Atomic force microscopy of the deformation region reveals increasing shear band heights with load, consistent with nanoindentation results. Whereas the spacing between semicircular shear bands was found to be independent of their distance from the tip of the indenter for the as-cast alloy, it was found to increase linearly, after a small zone of constant spacing, in the annealed alloys. Implications of this study in understanding the mechanical behavior of metallic glasses and their derivatives are discussed.

Keywords: Bulk amorphous materials; Hardness; Plastic deformation; Shear bands; Crystallization

1. Introduction

Indentation tests are an excellent means of conducting studies on elasto-plastic behavior of materials, for gaining insights into the micromechanisms of plastic deformation, as well as developing an understanding of the material's response to multiaxial loading. Because of these advantages, the indentation response of amorphous metals has been extensively studied and modeled [1–14]. Results show that the metallic glasses exhibit relatively high hardness, often more than three times the compressive yield strength [12]. This work was initiated to critically examine the deformation morphology associated with the Vickers indentation of as-cast and systematically crystallized $Pd_{42}Ni_{40}P_{18}$ bulk metallic glass (BMG) so as to identify the microscopic features that result in the high hardness of metallic glasses. Both bulk and interface Vickers indentation experiments, the latter employing the bonded interface technique, were conducted. Additionally, the influence of annealing treatments, which induce structural relaxation and partial crystallization, on the hardness and deformation behavior was investigated. The motivation for this study comes from the results of recent studies that show that annealing the as-cast bulk metallic glasses (BMGs) can markedly alter their mechanical behavior [14–17]. For example, it was shown that the partial crystallization, while marginally increasing the tensile fracture strength, could lead to a precipitous drop in the fracture toughness [15]. Fundamental understanding of the

* Corresponding author. Tel.: +91 80 2293 3241; fax: +91 80 2360 0472.
E-mail address: ramu@met.iisc.ernet.in (U. Ramamurty).

1359-6454/$30.00
doi:10.1016/j.actamat.2004.10.023

micro-mechanical reasons for this is far from complete. Since the stress, strain and displacement ahead of a sharp indenter and a crack are largely similar, further understanding of plastic behavior of annealed BMGs can be developed by studying the morphological characteristics of the indentation deformation zones with annealing.

2. Materials and experiments

The Pd-based ternary alloy with a nominal composition of $Pd_{42}Ni_{40}P_{18}$ was formed by melting pure metals in argon atmosphere and then chill-casting in a copper mould to produce 5 mm diameter BMG rods. The as-cast alloy was characterized using X-ray diffraction (XRD), differential scanning calorimetry (DSC), and transmission electron microscopy (TEM) to ascertain its amorphous nature. Relevant mechanical properties of the $Pd_{40}Ni_{40}P_{20}$ BMG (which is nominally similar in composition to that used in this study) are listed in Table 1.

To introduce partial crystallinity, the as-cast alloy samples (vacuum sealed in quartz tubes) were given isothermal annealing treatments at 350 °C for 10, 30 and 60 min, followed by water quenching. Also, one specimen was crystallized completely by annealing it at the same temperature for 300 min.

Specimens for the bonded interface technique were prepared by cutting the as-cast or annealed specimens first into two halves and then polishing them to a 1 μm finish prior to bonding the polished surfaces using a high strength adhesive. In order to minimize the bond layer thickness and to obtain a high strength bond, specimens were put into PVC moulds and then filled with cold mount resin. Following this, the top surface of the bonded specimen was polished carefully so that the indentation face is flat. Vickers diamond indentations were performed both on the bonded interface as well as away from it in the bulk. Indentations on the interface were conducted in such way that one of the indentation diagonals coincides with the interface [1]. The loads applied varied from 500 to 5000 g for the interface indentation whereas for bulk indentation (i.e., indentation away from interface) loads ranged from 50 to 2000 g. The bonded interface was opened subsequently by dissolving the adhesive in acetone. Deformation zones, both under the indenter tip (subsurface) as well as around the bulk indentations, were examined using a scanning electron microscope (SEM) and in selected cases atomic force microscope (AFM) and parameters like shear band spacing, plastic zone size, etc. were quantified.

Table 1
Elastic and mechanical properties of $Pd_{40}Ni_{40}P_{20}$

Property	Value	Reference
Young's modulus, E	108 GPa	[39]
Poisson's ratio, ν	0.40	[39]
Shear modulus, G	38.6	[39]
	36.6 GPa	[40]
Yield strength in compression, σ_{yc}	1.78 ± 0.08 GPa	[23]
Yield strength in tension, σ_{yt}	~1.6 GPa	[24]
Fracture strength in tension, σ_{ft}	~1.7 GPa	[24]
Average angle between slip plane and compression axis	41.9 ± 1.2°	[23]
	44	[24]
α (in Mohr–Coulomb yield criterion)	0.11	[2]
Brinnel hardness, H_B	551 ± 72 kg/mm^2	[3]
Vickers hardness, H_V	538 ± 16 kg/mm^2	[3]

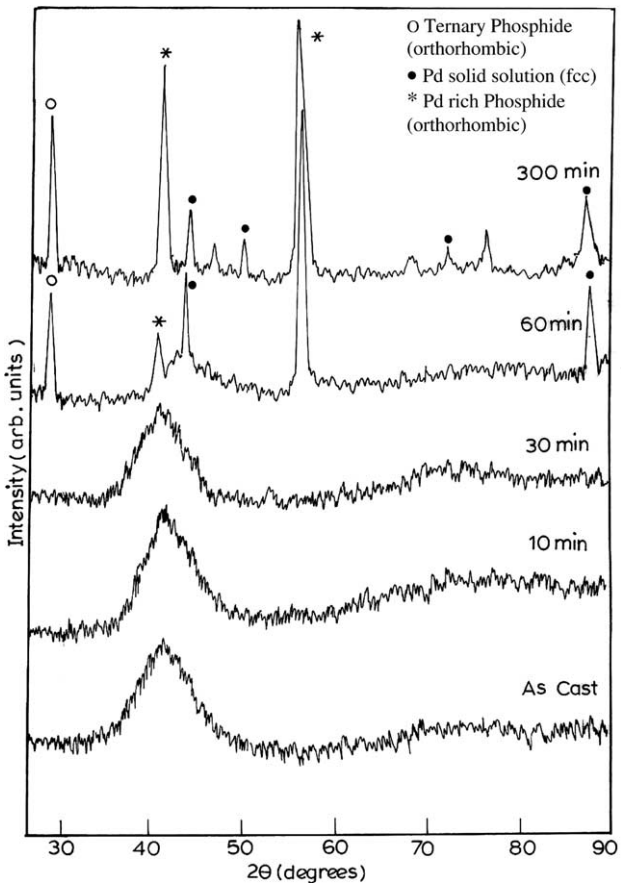

Fig. 1. X-ray diffraction patterns of the as-cast and annealed $Pd_{40}Ni_{40}P_{20}$.

3. Microstructural characterization

Fig. 1 shows the XRD patterns obtained from the as-cast and the heat-treated samples. The as-cast alloy exhibits a diffuse halo, characteristic of a glassy struc-

[1] We have also performed some control tests with the indentation diagonal perpendicular to the bonded interface. The morphological features are similar to those seen in the case where the diagonal is parallel.

ture. Annealing at 350 °C for up to 30 min does not change the XRD pattern significantly; the broad peak appears to get marginally sharper but no crystalline peaks are seen. Diffraction peaks indicating prominent crystallization, superimposed on a diffuse scattering hump that spans ~35–50°, appear in the sample which was heat treated for 60 min. In the sample that is fully crystallized, sharp and distinct peaks without any background diffuse hump are seen. On heat treatment, the ternary phase of Pd–Ni–P with an orthorhombic structure ($a = 0.41$ nm, $b = 0.64$ nm and $c = 0.785$ nm) evolves as the most prominent phase. In addition, the peaks corresponding to the Pd–Ni solid solution as well as weaker lines of Pd-rich phosphide are also observed.

The DSC thermogram of the as-cast alloy indicates that the glass transition temperature, T_g, is 295 °C and a supercooled liquid region that spans ~80 °C before the onset of crystallization at 374 °C. The TEM images obtained from the as-cast and 10 min annealed alloys were featureless. In the 30 min annealed alloy, sharp and continuous crystalline rings as well as an amorphous halo are seen in the selected area diffraction pattern (Fig. 2(a)). The sharp rings can be indexed in terms of an fcc structure with the estimated interplanar spacings matching with those of a Pd–Ni solid solution. The DF image, taken with the aid of the third ring in the diffraction pattern, confirms the presence of very small (~5–10 nm) crystalline domains embedded in an amorphous matrix. However, annealing for longer periods results in a heterogeneous microstructure consisting of very large-sized eutectic phases embedded in a nanocrystalline matrix. Fig. 2(b) is an optical micrograph of the BMG heat treated for 60 min, showing the spherulite nodules of the eutectic reaction product. A bright field TEM micrograph of the matrix is given in Fig. 2(c), which reveals a nanocrystalline structure with grains that are ~30 nm in diameter and ~100 nm in length. Upon further annealing, a fully crystalline material with a spherulitic microstructure is obtained. These results are consistent with those reported earlier in the literature [18–20].

4. Bulk indentation

4.1. Hardness

Fig. 3 shows the variation of hardness, H (calculated on the basis of the projected area of the indenter

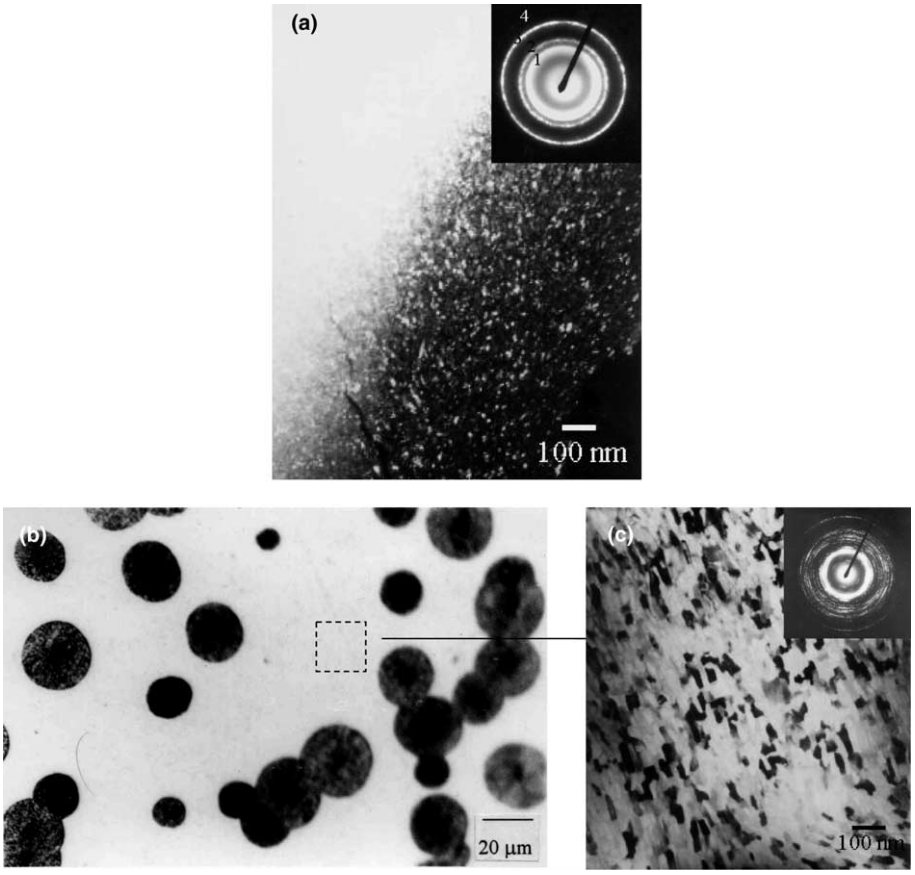

Fig. 2. (a) Dark field TEM micrograph of the 30 min annealed $Pd_{40}Ni_{40}P_{20}$; (b) an optical micrograph of the 60 min annealed $Pd_{40}Ni_{40}P_{20}$; and (c) a bright field TEM image obtained from the matrix region.

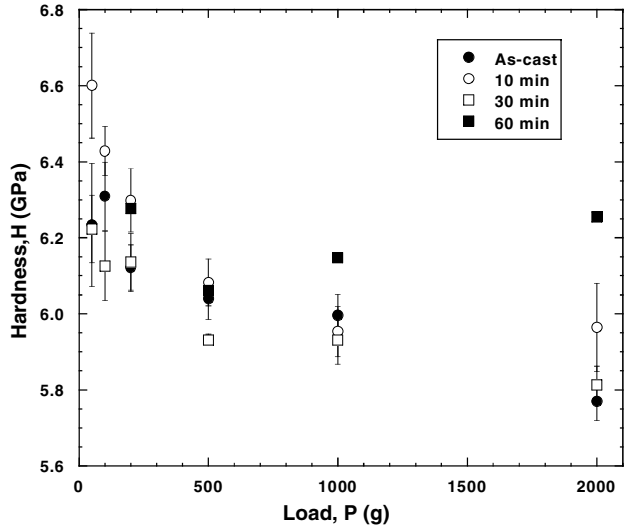

Fig. 3. Hardness, H, vs. load, P, plot for the as-cast and the annealed $Pd_{40}Ni_{40}P_{20}$.

impression), as a function of the indentation load, P. For the as-cast, 10 and 30 min annealed alloys, the average H values are marginally higher (in the range of 6.1–6.3 GPa) for loads below 500 g. Above 500 g, H is in the range of ~5.8–6 GPa, comparable to the 540 kg/mm^2 of H obtained by Davis [1] and 551 ± 71 kg/mm^2 obtained in spherical indentation by Donovan [3], for a similar alloy. Donovan reports a higher H in the lower load range of 30–50 N as compared to a slightly lower H (lower by ~15%) within the indentation load range of 100–359 N, a trend that is consistent with the Vickers indentation results of the current study. Absence of shear band coronets (due to pile-up of the material around the indents), which are otherwise common features around the indents made at high loads, and presence of shallow laterals crack at low loads (in addition to the radial cracks that are observed throughout the loading) were reported by Donovan. In the present study, despite the similarity in the alloy composition as well as the load range probed with that of Donovan, no cracking was observed in the as-cast BMG either at the indent corners or in the subsurface. Furthermore, shear bands were observed around all the Vickers indents irrespective of the load. These observations rule out the possibility of subsurface cracking as a reason for the higher H measured at low loads in our study.

Wright et al. [4] have conducted nanoindentation experiments on a $Zr_{40}Ti_{14}Ni_{10}Cu_{12}Be_{24}$ BMG and observe a higher H at low depths of penetration (<200 nm), possibly a result of finite radius of curvature (234 nm) of the Berkovich indenter tip that they have used. Lam and Chong [7] observe a similar behavior to that of Wright et al. [4] and attribute it to the indentation size effect. However, it is unlikely that such an effect is the reason for the observed H vs. P variation in this study as (i) the indentation loads used (even the smallest of them) are very large and (b) the higher H in the low load regime is only marginally larger (~10%). If indentation size effect was to be the cause, a large increase (~50%) in hardness at low loads can be anticipated. It is possible that the high H values at low loads are due to experimental artifacts such as a slightly rounded indenter tip affecting the hardness measurements at those loads.

The hardness of a metallic material is often related to its yield strength under uniaxial compression, σ_y, through the relation [21]

$$\sigma_y = H/C, \tag{1}$$

where C is the normalized hardness (also referred to as the constraint factor) that depends on the σ_y/E and H/E ratios as well as the shape of the indenter [22]. Donovan [23] measured σ_y to be ~1.78 GPa by compression testing 2 mm diameter $Pd_{40}Ni_{40}P_{20}$ alloy samples. Note that this value is larger, by ~10%, than the measured values of 1.6 GPa reported by Mukai et al. [24], who have conducted uniaxial tensile tests on 2.5 mm diameter specimens made from a BMG of same nominal composition. This difference in tensile and compressive yield strengths is due to the pressure sensitivity of deformation in BMGs [25]. Using 1.78 GPa for σ_y and 5.77 GPa for H for the as-cast alloy (the latter measured at an indentation load of 2000 g), a value of ~3.2 for C is obtained, which is consistent with that reported for Pd-based glasses by Sargent and Donovan [2] and Golovin et al. [6]. Note that detailed numerical simulations that incorporate large-scale plasticity show that the maximum value of C can be 2.75 for Vickers indentation [26]. A value for C that is greater than 3 suggests a pressure sensitivity for deformation.

Patnaik et al. [12] have analyzed the spherical indentation response of metallic glasses using finite deformation, finite element procedure that incorporates an extended Drucker–Prager material model (which is similar to that Mohr–Coulomb yield criterion) and report that the constraint factor depends on the indentation strain. It was shown that C increases strongly with the pressure sensitivity, particularly at large strains. The higher hydrostatic pressure that prevails underneath the indenter in pressure sensitive solids is the primary cause for this behavior. A limiting value of ~3.5 is obtained for the Mohr–Coulomb parameters of Zr- and Pd-based BMGs reported in literature. These observations are consistent with those made on the basis of the H measurements of the present study.

Turning to the H variation with annealing time, for loads higher than 500 g, H appears to decrease initially upon annealing for 10 min at 350 °C and then increase with increasing annealing time. An increase in H with the annealing time at temperatures above the T_g has been reported for a wide variety of BMGs [17]. In most cases, the hardness increase is linear with the crystalline

volume fraction and is attributed to the micromechanism of nanocrystalline phase resisting what is otherwise unhindered propagation of shear bands (in a manner similar to that offered by precipitates to dislocations in Al alloys upon aging) [27]. It is also suggested that solute enrichment in the amorphous phase due to primary crystallization can be the mechanism responsible for the continuous increase in the hardness even when the crystalline phase is softer as in the case of Al–Ni–Y alloys [27].

4.2. Deformation zone around the indents

Fig. 4(a) shows a representative indentation image obtained from the as-cast alloy indented with a 2000 g load. Pile-up of the material in the form of semi-circular shear bands is seen. These bands appear to emanate from the edge of the indentation and are wavy in nature as illustrated with a tilted high-magnification image of an indent edge shown in Fig. 4(b). It is seen from Fig. 4(b) that these are not cracks but are overlapping layers of upwardly displaced material. Owing to the volume conserving nature of the plasticity, deformation in elastic-perfectly plastic solids occurs by the pile-up of the material against the faces of the indenter. This pile-up is seen as discrete steps in the case of BMGs because of the inhomogeneous nature of plastic deformation in them.

Patnaik et al. [12] observe the included angle between two families of shear bands emanating from the edge of a spherical indent in a Zr-based BMG to be ~79°. Note that the included angle between the maximum shear directions would be 90° if the material obeys von Mises yield criterion. Fig. 4(b) indicates that the angle between the normal to the edge of the Vickers indent and the shear band tangent is about 30° as against 45° that expected for a Mises solid. Again, this observation implies strong pressure sensitivity for the plastic deformation in $Pd_{42}Ni_{40}P_{18}$.

Shear banded pile-up regions were observed in the samples that were heat treated up to 30 min for all the loads examined. Cracking was observed in the 60 min annealed alloy, as shown in Fig. 4(c), which is subjected to a load of 1000 g. Note that while cracking at one corner and chipping at an adjoining edge are seen in this image, the other three edges show features that are similar to that seen in the as-cast alloy. This is possibly due to the duplex microstructure of nanocrystalline matrix with relatively large spherical crystallites seen in the 60 min annealed alloy. When the indentation was made on an area that is nanocrystalline, the deformation morphology is similar to that seen in the as-cast or shorter-period annealed $Pd_{42}Ni_{40}P_{18}$. On the other hand, when the indentation happens to be on the relatively coarse globular particles or one of the indenter edges 'interacts' with them, cracking is seen indicating these intermetallic phases are highly brittle. Fig. 4(d) shows extensive cracking emanating from the corners of a Vickers indent made in a fully crystallized alloy sample indented with only a load of 200 g, confirming the extremely brittle nature of the alloy in this state. Because of this cracking, it was not possible to make reliable hardness measurements in the fully crystallized alloy and hence further studies on it were not pursued.

A plot of the shear band zone size, δ (measured as the distance between the center of the indent to the

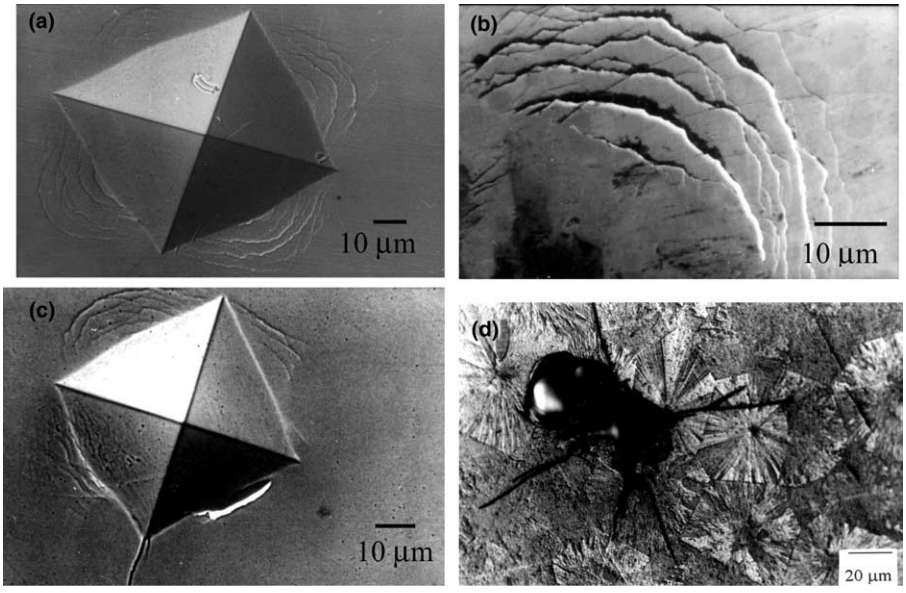

Fig. 4. SEM images of the indentations in: (a) the as-cast (P = 2000 g); (b) higher magnification image of (a) showing the shear band morphology; (c) 60 min annealed (P = 1000 g); and (d) fully crystallized $Pd_{40}Ni_{40}P_{20}$ (P = 200 g).

outermost shear band), vs. indentation load, P, for the as-cast and annealed $Pd_{42}Ni_{40}P_{18}$ is shown Fig. 5. As seen, δ increases with P and the trends in all cases are best described by a $\delta \propto P^{0.5}$ fit, with the regression coefficients, R either close to 0.99 or better. As tabulated in Fig. 5, the value of the proportionality constant C_1 is close to 1.1 for all the alloys except for the 10 min annealed alloy, consistent with the lower hardness measured in that condition.

Starting with Johnson analysis [22] of the stresses in the plastic region in the expanding spherical cavity model of an elastic–plastic material underneath an indenter and assuming that only the radial stresses carry the indentation load, Kramer et al. [28] have shown that the plastic zone size is related to the materials yield strength through the following relation:

$$\delta = \left[\frac{3P}{2\pi\sigma_y}\right]^{0.5}. \tag{2}$$

Validity of the above equation was experimentally verified on a wide variety of metals (both in single- and in poly-crystalline form) at macro-, micro-, and nano-scopic levels [28]. A few exceptions, such as the single crystals of tungsten and zinc indented using a nanoindenter, were argued to be a result of the indentation size effects and/or severe strain hardening effects.

The functional relationship predicted by Eq. (2) is obeyed by the $Pd_{42}Ni_{40}P_{18}$, both in the as-cast and annealed conditions. This implies that the expanding cavity model in general can be used to describe the plasticity in BMGs underneath the indenter. By setting C_1 equal to $[1.5/(\pi\sigma_y)]^{0.5}$, a value of ~2813 MPa is extracted for σ_y, which is considerably higher than the experimental value of ~1.8 GPa. Alternatively, Eq. (2) predicts a plastic zone of 72 μm for the as-cast alloy at P = 2000 g for a σ_y = 1.8 GPa whereas the measured value of δ at that P is ~44 μm.

Giannakopoulos et al. [29] have performed a comprehensive analysis of Vickers indentation through FEM simulations and conclude that, for elasto-plastic contact in nonhardening solids, $C_1 = [0.3/\sigma_y]^{0.5}$, indicating that the Johnson's model overestimates the plastic zone. Using this result, we obtain σ_y of 2522 MPa, which is still 40% higher than that measured in experiments by Mukai et al. [24]. Conversely, the estimated plastic zone size at 2000 g load is 57 μm, about ~30% higher than the experimentally measured value.

For sharp indentation of metallic materials, Johnson [22] derived the normalized plastic zone size, δ/a (where a is the contact radius), as

$$\frac{\delta}{a} = \left[\frac{E\tan\beta}{6\sigma_y(1-\nu)} + \frac{2}{3}\left(\frac{1-2\nu}{1-\nu}\right)\right]^{1/3}, \tag{3}$$

where ν is the Poisson's ratio, and β is the cone angle. As per Eq. (3), δ/a does not depend on P, a result of the self-similarity of stress and strain fields for geometrically similar indenters.

For the Pd-based BMG, when δ is normalized with the diagonal of the Vickers indent, D, and plotted as a function of P (Fig. 6), it is seen that δ/D indeed remains approximately constant at about 0.55. Using the literature values for E, ν, and σ_y (Table 1), an equivalent contact angle (in order to get the same volume of material displaced in cone and Vickers indentations [27]) of 19.7° and scaling the resulting δ/a (by setting the projected contact areas for Vickers and cone indentations

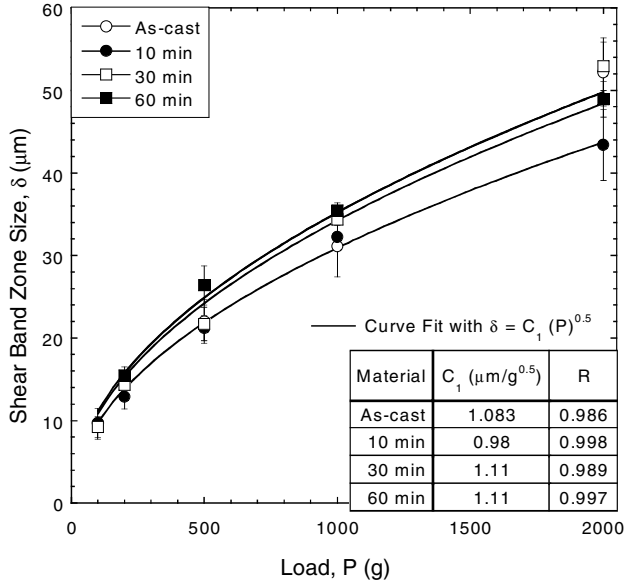

Fig. 5. Shear band zone size, δ, vs. load, P, for the as-cast and annealed $Pd_{40}Ni_{40}P_{20}$.

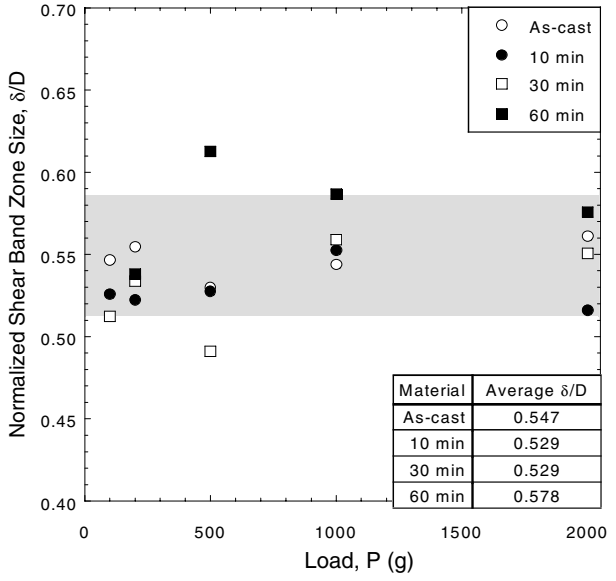

Fig. 6. Variation of the normalized shear band zone size, (δ/D) with the load, P.

equal), we get a δ/D of ~0.73, which is again higher by ~30%, than the measured value.

In summary, the trends in the experimental data obtained by indenting the BMGs are in accordance with those predicted theoretically and also validated experimentally for indentation of crystalline metals. However, the extracted σ_y are markedly different from those measured in uniaxial compression and indicate that the existing theories either overestimate the plastic zone size or the true δ may be larger than what is measured, by about 30–40% in both the cases. Possible reasons for these discrepancies are elaborated below.

- Underestimation of the plastic zone size. Note that shear bands are the result of intense plastic deformation. Hence δ, while giving a measure of the plastic zone size, underestimates the elasto-plastic boundary. It is also likely that the SEM imaging technique used in the present study to estimate δ could not capture the finer shear bands that may be lying at the periphery and hence the actual plastic zone size can be much larger than δ. In this context, it is interesting to note that the plan view contours of the effective stress, obtained by Vaidyanathan et al. [5] using FEM simulations (see Fig. 9 in Ref. [5]), indicate a larger plastic zone size vis-à-vis the experimentally observed shear band zone size.
- The expanding spherical cavity model, on the basis of which Eqs. (2) and (3) have been derived, while sufficient to predict the trends, does not incorporate certain features that are salient to the deformation of metallic glasses. For example, the Johnson model [22] or the analysis of Giannakopoulos et al. [29] either implicitly or explicitly assumes that only the deviatoric stress causes yielding. However, the hydrostatic stress also affects the plastic deformation of amorphous metals and hence needs to be considered. Hence, it is likely that these models are overestimating the plastic zone size in the BMGs. This is also evident from the numerical simulations of the P–h curves, which shows a larger residual depth of penetration when von Mises yield criterion is used as compared to that obtained using the Mohr–Coulomb yield criterion [5,12].
- The process of plastic deformation through shear bands is a discrete phenomenon and also inhomogeneous in nature whereas continuum models consider homogeneous plastic deformation that occurs smoothly. Molecular dynamics simulations suggest that the shear band nucleation process strongly depends on the distribution of the free volume and hence the deformation behavior of BMGs can be highly stochastic, at least locally [30]. Naturally, these subtle effects have to be built in to a model that captures the experimental results accurately.

5. Subsurface deformation

As mentioned in the introductory section of this paper, Donovan [3] has attempted to study the geometry of plastic flow in the $Pd_{40}Ni_{40}P_{20}$ amorphous metal indented with Brinell and Vickers indenters. For this purpose, she has employed sectioning, polishing, and etching of the polished surfaces successively and reported that the shear bands etch lightly and hence were seen only as faint lines. This makes the resolution of the individual slip lines with good contrast and distinguishing them with the polishing scratch lines difficult. Additionally, cracks that were otherwise absent in the as-polished sections are seen extensively in the etched sections, indicating that they are probably a result of stress corrosion cracking. Fracture toughness values estimated from the indentation cracking are lower than those typical of metallic glasses, confirming that cracks seen after etching are incipient cracks than fully developed ones. These observations of Donovan [9] indicate that an alternative technique is needed for examining the subsurface deformation behavior of BMGs. The bonded interface technique, which has been widely used to study the subsurface deformation and plastic flow during indentation of ceramics and glasses, is an alternative. While the advantage with this technique is the ability to image the deformation morphology (especially for the metallic glasses which undergo inhomogeneous deformation), it suffers from the fact that the adhesive layer relieves the elastic constraint for plastic flow that otherwise would be present in a semi-infinite block indentation. This can potentially introduce changes to the size and shape of the deformed zone as well as alter the deformation mechanism itself. Samuels and Mulhearn [31], Mulhearn [32] and Dugdale [33] have conducted extensive studies to examine this possibility and conclude that differences in the deformation characteristics of the material may affect the extent of the deformed zone and the slope of the strain gradient but have no significant effect on the contours of equal strain.

We have conducted experiments to examine if there is significant effect of the relaxation of the constraint due to the presence of a compliant interface on the size and morphology of the subsurface deformation zones. For this purpose, the polished pieces of the BMG were held together in a vice. The application of mechanical force (as against the adhesive) prevents the separation of the two mating blocks during indentation. Observations reveal insignificant differences between those held together by adhesive bonding and those by mechanical force.

5.1. Morphology

Fig. 7(a) shows the plan view of the deformed region underneath a Vickers indent (5000 g load) in the as-cast

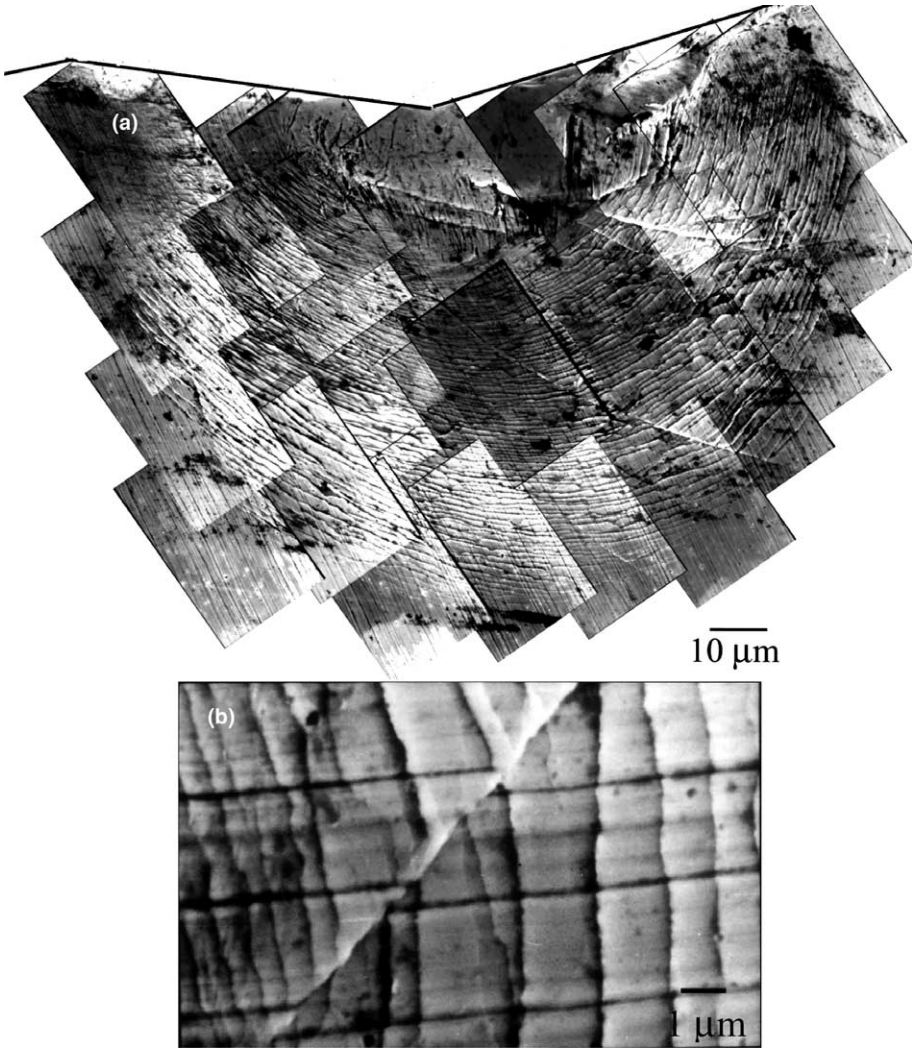

Fig. 7. (a) Plan-view of the SEM images obtained from the subsurface deformation zone in the as-cast $Pd_{40}Ni_{40}P_{20}$ (P = 5000 g), obtained using the bonded interface technique, highlighting the shear band morphology underneath the indenter. (b) A higher magnification image obtained from within the deformed region of (a).

BMG, which is semi-circular in shape containing a high density of shear bands. No cracks were observed within the deformed zone. Close to the indenter tip, a small zone (~10 μm in size) that is relatively free of any shear bands is observed. Within the deformation zone, two morphologically distinct shear bands are seen, semi-circular and radial. The density of the semi-circular shear bands is considerably larger. Tilting in the SEM reveals the hemispherical deformed zone is a result of the plastic flow of the BMG into the interface (which is about ~5 μm thick). The relaxation of constraint due to the presence of a highly compliant interface that has a finite thickness (~5–10 μm) facilitates for the plastic flow of the material into the interface as against the flow-up seen in the bulk indentation. Because of the inhomogeneous nature of the plastic deformation in the BMG, the surface of the plastic bulge is not smooth but is serrated containing a number of discrete steps. These steps appear as semi-circular shear bands in the plan view as seen in Fig. 7(a). Note also that the shear bands at the edges of the Vickers impression on the indented surface are not present in the case of the bonded interface, as material flow against the indenter faces is not necessary.

While the semi-circular shear bands are out-of-plane (plane stress) shear displacements, the radial bands are a result of the in-plane (plane strain) shear displacements. This is illustrated with a higher magnification image (Fig. 7(b)) from the deformed region that shows polishing scratch marks (horizontal lines) displaced by a radial shear band. Note that the semi-circular shear bands (seen as near vertical lines) do not appear to distort or displace the scratch marks as this micrograph gives a plan view of the deformed region. Interestingly, the radial shear band displaces the semi-circular bands, indicating that the deformation through in-plane shear displacements occurs after out of plane deformation.

Two possible mechanistic scenarios for this can be construed. The first is that the radial bands form after the out of plane deformation reaches saturation. Alternatively, the radial bands could have formed during unloading because of the reverse plastic flow caused by the elastically strained matrix. Because of the compliant interface, the elastic constraint of the surrounding matrix is likely to be insignificant and hence the first mechanism is more likely to be the case.

Note that the results obtained by Donovan [3] represent those under the plane strain condition (as there will not be any out of plane displacement of the material in the absence of an interface), the results obtained using the bonded interface technique represent deformation under plane-stress conditions.

AFM was conducted on the as-cast alloy indents to study the finer details of subsurface deformation zone as well as to confirm that the deformation morphology observed is indeed due to shear band formation and not cracking. Fig. 8(a) shows an AFM image of the subsurface region of a 2500 g Vickers indent. The radial bands are seen more clearly from this image. Closer examination of the topology, Fig. 8(b), reveals the substructure of the shear bands. Several parallel fine lines within a major shear band indicate that at microscopic scale each band is a composite of few finer shear bands. Furthermore, the shear bands seem to have formed by joining several ellipsoids of different heights together. This feature indicates that shear band propagation within the material is not very smooth, but tortuous or wavy in nature.

Analysis of the AFM line scans was performed in order to quantitatively measure the surface roughness and in turn estimate the shear displacements associated with the propagation of shear bands. A typical line scan, obtained from the 2500 g indent, is shown in Fig. 8(c). The average RMS values (which is a reflective of the shear band height) obtained from such data are plotted in Fig. 8(d) as a function of P. It is seen that the average shear band height varies linearly with P; between 25 and 45 nm. Golovin et al. [6], who have observed serrated flow during instrumented indentation of a $Pd_{40}Cu_{30}Ni_{10}P_{20}$ BMG alloy, show that the span of the horizontal displacement jump (a consequence of the shear band nucleation and propagation) to vary between 10 and 40 nm. Schuh and Nieh [9,11], who have studied the rate effects on the indentation behavior of several BMGs, report an increase in the pop-in depth with increasing depth of penetration, reaching a value of ~15 nm at ~300 nm depth of penetration for the $Pd_{40}Cu_{30}Ni_{10}P_{20}$ alloy. Both these observations are generally consistent with the average shear band height observed in the present study, keeping in view that (i) the loads applied are significantly larger and (ii) each microscopic shear band is a composite of few finer shear bands.

The SEM micrographs of the subsurface deformation regions in the 10, 30 and 60 min annealed alloys are

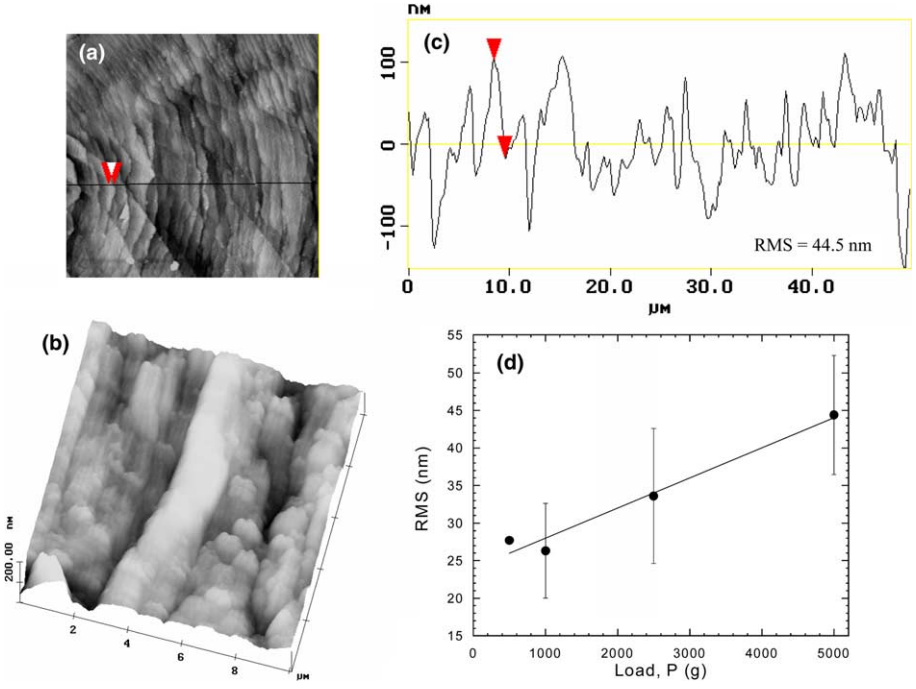

Fig. 8. (a) AFM image obtained from the subsurface deformed region of the as-cast $Pd_{40}Ni_{40}P_{20}$ (P = 2500 g). (b) Higher magnification image from (a) showing the finer structure of the shear bands. (c) Line scan from (a) showing the displacements associated with shear bands. (d) Variation of the average root mean square (RMS) values of the surface roughness with indentation load, P.

shown in Fig. 9(a), (b), and (c), respectively. In both the 10 and the 30 min annealed samples, the deformation zone is devoid of cracks with a shape that is similar to that seen in the as-cast alloy. However, a gradual transition in the shear band morphology, from a near-complete semi-circular band dominated process zone in the as-cast alloy to a process zone where both types of bands are equally prominent, is seen. Another qualitative observation is that the waviness in the shear bands appears to decrease with increasing annealing time.

In the 60 min annealed alloy, however, extensive cracking interspersed with shear band deformed regions is seen, as shown in Fig. 9(c). The cracks appear to encircle the larger spherical crystalline phase whereas the shear band deformation occurs in the nanocrystalline regions. Wei et al. [34] have shown that the governing mechanism of plastic deformation in nanocrystalline Fe is also shear banding. In light of their results, it is not surprising to see that the matrix of the 60 min alloy, which is nanocrystalline, deforming extensively through shear banding. However, the large crystalline phases are typically intermetallic in nature and hence cannot accommodate plastic strains. As a result of this plastic mismatch between the matrix and the crystalline phases, cracking around the latter occurs.

The spacing between semicircular shear bands, φ, is plotted as a function of distance from the tip of the indenter impression, ξ, for the as-cast and 10 and 30 min

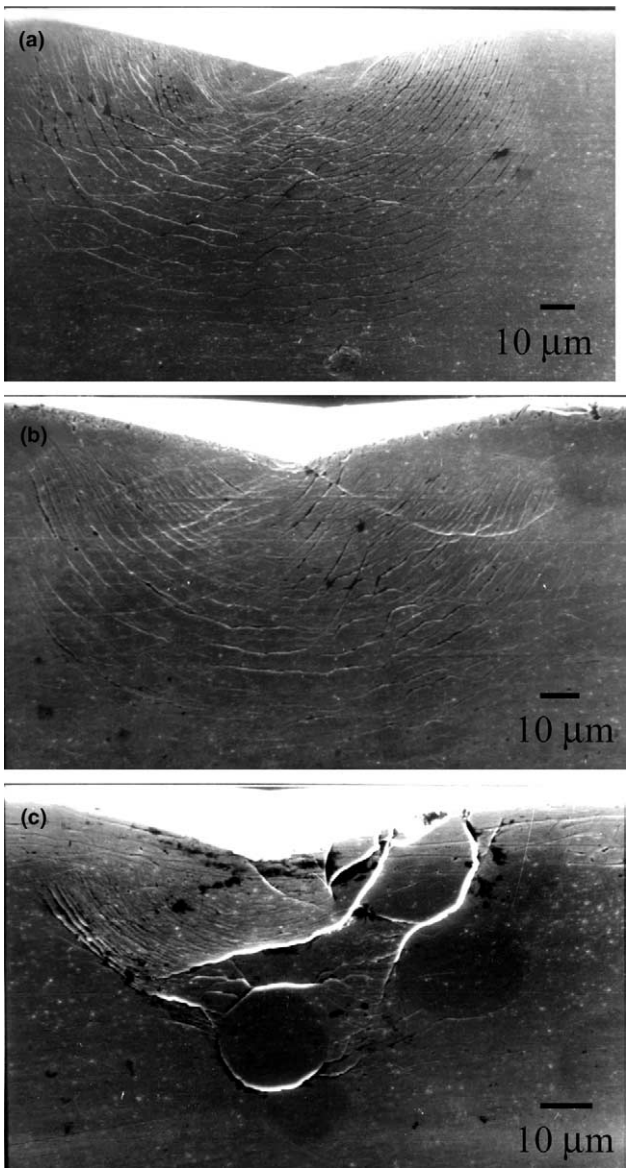

Fig. 9. SEM images of the subsurface deformation regions obtained in (a) 10 min and (b) 30 min annealed (P = 5000 g for both), and (c) 60 min annealed $Pd_{40}Ni_{40}P_{20}$ (P = 2500 g).

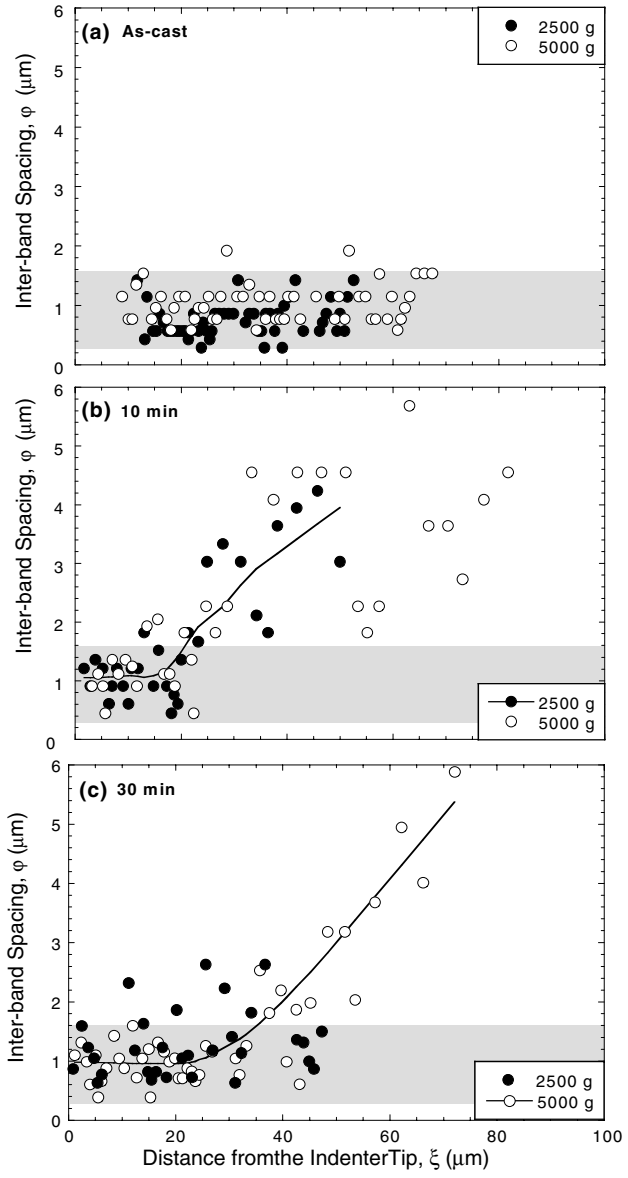

Fig. 10. Variation of the distance between adjacent shear bands, φ, as a function of their distance from the tip of the indentation impression, ξ, for the (a) as-cast and (b) 10 and (c) 30 min annealed $Pd_{40}Ni_{40}P_{20}$.

annealed alloys in Fig. 10(a)–(c). For the as-cast alloy, φ is constant and independent of ξ, with an average spacing of ~1 μm. However, φ is ~1 μm in a zone close to the indenter tip for the 10 and 30 min annealed alloys. This zone size is ~20 and 40 μm for the 10 and 30 min annealed alloys, respectively. Beyond this zone, φ increases with ξ.

5.2. Deformation zone size

Fig. 11 shows the variation of the size of subsurface deformation zone, λ, as a function of P, both for the as-cast and annealed samples. For a given P and material condition, the λ values are similar to the corresponding δ values. For example, in the as-cast alloy and at $P = 1000$ g, λ ~37 μm whereas $\delta = 32$ μm. The trends in λ vs. P are similar to those seen in δ vs. P for bulk indentation and the relationship $\lambda = C_2(P)^{0.5}$ captures the trends reasonably well, with R values greater than 0.99 for all the cases. Because of the similarity in λ and δ, the range of values for C_2 is similar to the range of C_1 values, the latter extracted from the bulk indentation experiments. For example, for the as-cast alloy $C_1 = 1.083$ whereas $C_2 = 1.09$. This observed similarity reinforces the utility of the bonded interface technique as a means to study the deformation behavior of materials.

However, a closer examination reveals some contrasting behavior, particularly for the 10 min annealed alloy. The δ value in this case is the lowest among the four material conditions examined and as a result C_1 also is lowest. In contrast, λ and hence C_2 are highest among those measured. Clearly, the relaxation of the constraint at the interface and hence prevalence of a plane-stress

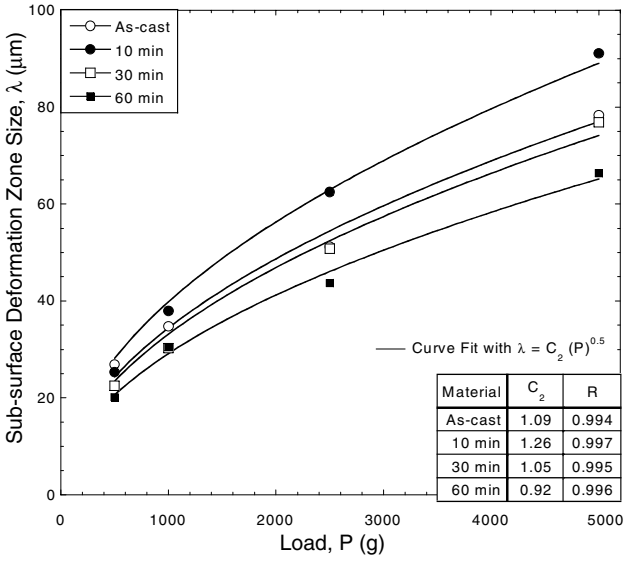

Fig. 11. Subsurface deformation zone size (i.e., distance from the indenter impression tip to the farthest shear band), λ, as a function of the indentation load, P.

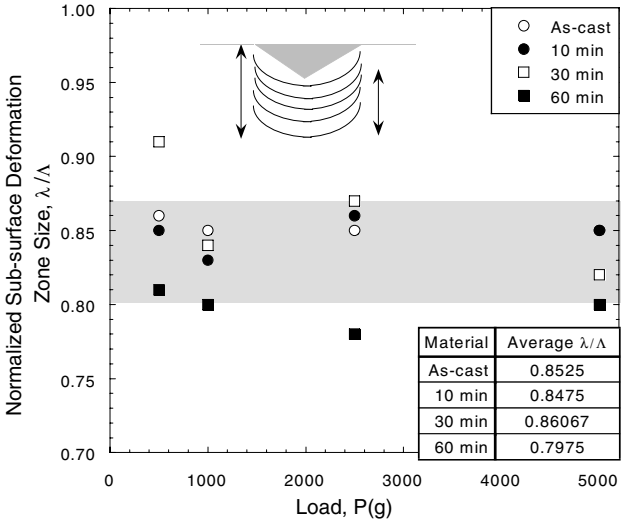

Fig. 12. Variation of λ normalized with Λ (total plastic zone size) as a function of P.

state coupled with some intrinsic change in the material deformation characteristics (such as the deviation from the elastic, perfectly plastic behavior) could be possible causes for this behavior. Mechanistic reasons for the 10 min annealed alloy's contrasting behavior are not yet clear.

Fig. 12 shows the variation in λ, normalized with $\Lambda(=\lambda + h$, where h is the depth of penetration) as a function of P. Most of the λ/Λ data falls within the range of 0.8 to 0.87, implying that it is independent of P. Average values of λ/Λ are listed in the inset table in Fig. 12. As seen, the as-cast, and 10 and 30 min annealed samples have a similar value of λ/Λ at around 0.85. While this value appears to be significantly larger than the λ/D, it has to be noted that the different normalizing parameters lead to this difference.

5.3. Discussion

A central idea of the expanding cavity model, developed by Johnson [22], is that the hardness of elastic–plastic materials is governed by the single material parameter $(E/\sigma_y)\tan\theta$, where θ is the angle between indenter face and the undeformed specimen surface (19.7° for Vickers indenter). For the Pd-based BMG under investigation, its value is 21.7, within the range of validity for the expanding cavity model. The deformation morphology confirms to the concept of radial displacement of material away from the point of first contact, giving rise to a hemispherical elastic–plastic boundary. The material displaced by the penetration of the indenter is either accommodated by the elastic expansion of the surrounding material or in the pile up of the material around indenter, in case of bulk indentation. In the case of the indentations at the interface, plastic flow into the compliant interface is the main accommodating processes.

However, the σ_y predictions, made from the plastic zone sizes using the expanding cavity model, are considerably larger than those observed in uniaxial compression. This is found to be true for both the bulk indentation as well as the interface indentation. Given that the metallic glasses exhibit pressure sensitivity in their plastic flow and that high hydrostatic static stresses exist underneath the indenter, it is reasonable to expect the elevation of stress required for the plastic flow initiation during indentation. Lu and Ravichandran [35] have studied that plastic deformation behavior of a Zr-based BMG under multiaxial compression experiments by using the confining sleeve technique and on the basis of these results suggest that the plastic flow in BMGs is governed by a pressure-dependent Tresca criterion of the following type,

$$\sigma_y(P) = \sigma_{y,0} + \beta p. \tag{4}$$

Here, $\sigma_{y,0}$ is the flow stress under uniaxial loading, p is the hydrostatic pressure and β is the coefficient of pressure dependence. For the Zr-based BMG, Lu and Ravichandran [35] report that $\beta \sim 0.17$. Small strain finite element analyses of Vickers indentation by Giannakopoulos et al. [29] show that close to the indenter tip, the maximum compressive hydrostatic stresses for an elasto-plastic material with no strain hardening is $\sim 1.83\sigma_y$. As per Eq. (4), this hydrostatic stress translates into an elevation of the flow stress of ~550 MPa for a $\beta = 0.17$. This is broadly consistent (despite the approximate nature of the calculations) with the ~40% higher flow stress estimated made using Eq. (2) from the pile-up zone sizes of the bulk indentation data.

Further, the interband spacing of ~1 μm for the as-cast alloy is similar to 1–2 μm spacing reported by Lu and Ravichandran [35], who also show that the BMG can carry large plasticity, more than 10%, under confinement. Given that a strongly decaying strain gradient (radially away from the point of contact) exists in the indented solids, invariance of φ with ξ within the plastically deformed zone implies that the shear banding is independent of stress, provided the stress exceeds a critical value. This implication is consistent with the elastic-perfectly plastic continuum deformation behavior typically expected for metallic glasses. Conner et al. [36] have investigated the thickness dependence of shear band spacing in metallic glass specimens subjected to bending. Their results show that the spacing scales with the thickness, indicating that thinner sheets are likely exhibit greater bend ductility due to finer separation between the bands. The AFM results indicate a shear offset of ~50 nm (at 5000 g load), which implies that each coarse shear band (with a φ of 1 μm) can carry about 5% plastic strain. This implication is generally consistent with the Lu and Ravichandran's observation that a multiaxial state of stress promotes finer band separation (and hence larger ductility). It also corroborates with the Conner et al.'s implication that a small deformation zone (underneath the indenter) can accommodate large plastic strains because of the finely spaced shear bands.

It is instructive to relate the measurements on shear band spacing to those made during the nanoindentation of metallic glasses. Several research groups [6,9,13] report that the indentation load, P, vs. depth of penetration, h, curves are decorated with several discrete displacement bursts, which were identified to be associated with shear band initiation and propagation underneath the indenter. Further, it was noted that the magnitude of displacement jumps, Δh, increases approximately linearly with h. Schuh and Nieh [9] suggest that this linear relationship between Δh and h is simply due to the self-similarity associated with the deformation fields underneath a sharp indenter. They attribute the absence of such "pop-ins" at high rates of loading to an intrinsic transition in the deformation mode, from discrete to homogeneous plasticity. They suggest that at high rates, the absence of pop-in events is due to the operation of several shear bands at any given instance. Considering the fact that the rates of loading for the present set of indentations are very high (of the order of a μm/s), the observation of equally spaced coarse shear bands that contain within them several finer shear bands indicates to the simultaneous operation of multiple shear bands. On the other hand, Greer et al. [13] suggest that the increase in Δh as well as the spacing between the bursts with the h is due to increasing indentation strain, which implies that the spacing between the shear bands should increase with increasing distance away from the indenter tip. However, the observations made in the present study for the as-cast alloy clearly indicates that φ is invariant with ξ. We suggest that perhaps, the distance that the shear bands have to traverse from their nucleation sites to the surface of the specimen is the controlling parameter for Δh.

With respect to the annealed alloys, it is seen from Fig. 10 that the shear band number density (per unit chord length) is much smaller in the annealed alloys vis-à-vis the as-cast alloy. This is because of the smaller zone of intense shear deformation and increasing shear spacing out of it for the annealed alloys. A pertinent question to ask at this juncture is why is the shear band spacing in annealed alloys different? A possible answer lies in the fact that deformation through shear bands is nucleation dominated, i.e., they propagate instantaneously once they nucleate, which is probably getting affected by the annealing treatments. Spherical indentation studies, wherein it is possible to study the indentation response of a given material as a function of indentation strain, on a Zr-based BMG suggest that the number density of shear bands in an annealed alloy is considerably lower than that observed in the as-cast alloy [37]. Further, higher strains are required to be applied for the observation of shear bands. In the present

study, higher strains that prevail close to the Vickers indenter tip promote extensive shear banding and deformation saturates. On the other hand, far away from the indenter tip, since the strains are lower the shear band spacing increases monotonically.

The suggestion that annealing of the alloy reduces the propensity of deformation through shear banding also helps to explain their mechanical properties, especially the precipitous drop in their toughness. High toughness in the as-cast BMGs is derived by the extensive plastic shear deformation at the crack-tip [38]. However, because of the larger average shear band spacing in the annealed alloys, the energy absorbed within the plastic zone of the crack-tip decreases and hence leads to precipitous drop. Further modeling work is necessary for corroborating this hypothesis.

6. Summary

A systematic study on the plastic deformation associated with Vickers indentation hardness tests on the as-cast and annealed $Pd_{42}Ni_{40}P_{18}$ BMG reveals that in general the shear banded deformation regimes around the indents, although inhomogeneous in their very nature, obey the expanding cavity model's idea of a hemispherical plastic zone. While the plastic zone sizes, both in bulk as well as bonded interface indentations, were found to scale with the square root of the indentation load, their relative size was much smaller than that anticipated, due to the pressure sensitivity of plastic flow exhibited by metallic glasses. The short-term annealed samples (i.e., those that did not show any crystallinity) did not reveal any features that are markedly different from that of the as-cast BMG. The only difference observed is a smaller zone of intense plasticity (with equal shear band spacing) in the annealed alloys, indicating the absence of widespread plastic zone ahead of a crack-tip (whose deformation fields are analogous to those under a sharp indenter) as a possible cause for the embrittlement of BMGs upon annealing.

Acknowledgements

We are grateful to Drs. S. Kulinich and S. Bysakh of the National Institute for Materials Science, Tsukuba, Japan for their help in conducting the AFM and TEM, respectively. Many useful discussions with Drs. Y. Choi and M. Dao of MIT are acknowledged. Financial support for this work was provided by a Defense Research and Development Organization grant to IISc.

References

[1] Davis LA. Scripta Metall 1975;9:431.
[2] Sargent PM, Donovan PE. Scripta Metall 1982;16:1207.
[3] Donovan PE. J Mater Sci 1989;24:523.
[4] Wright WJ, Saha R, Nix WD. Mater Trans JIM 2001;42:642.
[5] Vaidyanathan R, Dao M, Ravichandran G, Suresh S. Acta Mater 2001;49:3781.
[6] Golovin YI, Ivolgin VI, Khonik VA, Kitagawa K, Tyurin AI. Scripta Mater 2001;45:947.
[7] Lam DCC, Chong ACM. Mat Sci Eng A 2001;318:313.
[8] Kim JJ, Choi Y, Suresh S, Argon AS. Science 2002;295:654.
[9] Schuh CA, Nieh TG. Acta Mater 2003;51:87.
[10] Jana S, Ramamurty U, Chattopadhyay K, Kawamura Y. Mater Sci Eng A 2004;375–77:1191.
[11] Schuh CA, Nieh TG. J Mater Res 2004;19:46.
[12] Patnaik MNM, Narasimhan R, Ramamurty U. Acta Mater 2004;52:3335.
[13] Greer AL, Castellero A, Madge SV, Walker IT, Wilde JR. Mater Sci Eng A 2004;375–77:1182.
[14] Fan C, Louzguine DV, Li C, Inoue A. Appl Phys Lett 1999;75:340.
[15] Nagendra N, Ramamurty U, Goh TT, Li Y. Acta Mater 2000;48:2603.
[16] Ramamurty U, Lee IML, Basu J, Li Y. Scripta Mater 2002;47:107.
[17] Basu J, Nagendra N, Li Y, Ramamurty U. Philos Mag 2003;83:1747.
[18] Donovan PE, Evans PV, Greer AL. J Mater Sci Lett 1986;5:951.
[19] Miller MK, Larson DJ, Schwarz RB, He Y. Mater Sci Eng A 1998;250:141.
[20] Lu IR, Wilde G, Görler GP, Willnecker R. J Non-Cryst Solids 1999;250–252:577.
[21] Tabor D. Hardness of metals. Oxford: Clarendon Press; 1951.
[22] Johnson KL. J Mech Phys Solids 1970;18:115.
[23] Donovan PE. Acta Metall 1989;37:445.
[24] Mukai T, Nieh TG, Kawamura Y, Inoue A, Higashi K. Scripta Mater 2002;46:43.
[25] Schuh CA, Lund AC. Nat Mater 2003;2:449.
[26] Dao M, Chollacoop N, Van Vliet KJ, Venkatesh TA, Suresh S. Acta Mater 2001;49:3899.
[27] Greer AL. Mater Sci Eng A 2001;304–306:68.
[28] Kramer D, Huang H, Kriese M, Robach J, Nelson J, Wright A, et al. Acta Mater 1999;47:333.
[29] Giannakopoulos AE, Larsson PL, Vestergaard R. Int J Solids Struct 1994;31:2679.
[30] Huang R, Suo Z, Prevost JH, Nix WD. J Mech Phys Solids 2002;50:1011.
[31] Samuels LE, Mulhearn TO. J Mech Phys Solids 1957;5:125.
[32] Mulhearn TO. J Mech Phys Solids 1959;7:85.
[33] Dugdale DS. J Mech Phys Solids 1955;2:14. and 265.
[34] Wei Q, Jia D, Ramesh KT, Ma E. App Phys Lett 2002;81:1240.
[35] Lu J, Ravichandran G. J Mater Res 2004;18:2039.
[36] Conner RD, Johnson WL, Paton NE, Nix WD. J Appl Phys 2003;94:904.
[37] Murali P, Ramamurty U. Acta Mater 2004 [submitted].
[38] Flores KM, Dauskardt RH. Mater Sci Eng A 2001;319–321:511.
[39] Lambson EF, Lambson WA, Macdonald JE, Gibbs MRJ, Saunders GA, Turnbull D. Phys Rev B 1986;33:2380.
[40] He Y, Schwarz RB. Mater Res Soc Symp Proc 1997;455:495.